Decays of $l = 1$ baryons: Quark model versus large N_c

Christopher D. Carone,* Howard Georgi,[†] Lev Kaplan,[‡] and David Morin[§]

Lyman Laboratory of Physics, Harvard University, Cambridge, Massachusetts 02138

We study hadronic two-body decays of the orbitally excited, SU(6) **70**-plet baryons in order to test the hypothesis that the successes of the nonrelativistic quark model have a natural explanation in the large-N_c limit of QCD. By working in a Hartree approximation, we isolate a specific set of operators that contribute to the observed s- and d-wave decays in leading order in $1/N_c$. We fit our results to the current experimental decay data, and make predictions for a number of allowed but unobserved modes. Our tentative conclusion is that there is more to the nonrelativistic quark model of baryons than large N_c.

PACS number(s): 13.30.Eg, 11.15.Pg, 12.39.Jh

I. INTRODUCTION

In the nonrelativistic quark model (NRQM), the baryon resonances can be classified by their transformation properties under nonrelativistic SU(6) spin-flavor symmetry. The ground-state baryons have completely symmetric spin-flavor wave functions, and form the 56-dimensional representation. The $l = 1$ orbitally excited states have spin-flavor wave functions with mixed symmetry that lie in the **70**. While the NRQM description of the baryon states has not been derived convincingly from QCD, it has been incorporated with some success in many of the previous theoretical attempts to understand the observed baryon masses and decay widths [1].

Recently, Dashen, Jenkins, and Manohar suggested an interesting interpretation of the approximate spin-flavor symmetry of the NRQM [2,3]. Working in the large-N_c limit, where N_c is the number of colors, they showed that the symmetry structure of the baryonic sector of QCD is constrained by the condition that pion-baryon scattering amplitudes remain finite as $N_c \to \infty$, so that unitarity is preserved. Exploiting these large-N_c consistency conditions, they were able to classify symmetry-breaking corrections to the mass and decay relations by their order in the $1/N_c$ expansion. They observed that the approximate NRQM spin-flavor structure of the $l = 0$ baryons in the SU(6) **56** could be understood as a consequence of large N_c, for baryons with small total spin. The analogous relations involving baryon states with spins of order $N_c/2$, however, are subject to large corrections.

Attempts to understand large-N_c baryon phenomenology more directly in terms of quarks and QCD appeared shortly afterwards in Refs. [6,7]. Reference [6] demonstrates that the connection to quarks follows from the ideas of Witten (see [8]), who showed that large-N_c

baryons can be treated in a Hartree approximation. In this picture, each quark in the baryon experiences an average potential generated by the other $O(N_c)$ quarks. In baryons with small total spin, each quark wave function corresponds to the same s-wave ground state. In baryons of higher spin, however, the spin-spin and spin-orbit interactions might significantly deform the quark wave functions away from the s wave. Reference [6] shows that this physical picture is consistent with the results of Dashen, Jenkins, and Manohar. The Hartree potential, at least in principle, can be computed using the part of the multiquark Hamiltonian that transforms trivially under spin and spatial rotations acting separately on each of the quark wave functions. The remaining piece of the Hamiltonian can then be included perturbatively. In this formulation of the problem, the spin-flavor symmetry appears at lowest order in the $1/N_c$ expansion, and the corrections are suppressed by powers of S/N_c, where S is the baryon spin. Again, the approximate spin-flavor symmetry can be understood as a consequence of large N_c, for baryons with small total spin.

One of the difficulties with the large-N_c picture of baryons is that the spin and flavor structure of the large-N_c baryons is not simply related to the spin and flavor structure of the $N_c = 3$ baryons, because the number of quarks is not the same. This has caused considerable confusion in the literature. Part of the value of the Hartree picture is that it suggests a calculational scheme for applying large-N_c ideas to the observed baryon resonances with $N_c = 3$ [6]. The first step is to categorize the relevant multiquark operators by their order in the $1/N_c$ expansion. This is not completely trivial, since an operator that is summed over the $O(N_c)$ quarks in the baryon state may have an effect that is as important as that of an operator that is formally of lower order, if the terms in the sum add coherently. Assuming that we have isolated the correct set of multiquark operators, we can then apply them to the baryon states, *defined with $N_c = 3$*. In this way, we avoid the problem of extracting our predictions from large-N_c baryon wave functions, which have quantum numbers that are different from those of the

---

*Electronic address: carone@huhepl.harvard.edu
[†]Electronic address: georgi@huhepl.harvard.edu
[‡]Electronic address: kaplan@huhepl.harvard.edu
[§]Electronic address: morin@huhepl.harvard.edu

baryons in the real world.

In this paper, we show how to apply these ideas to hadronic decays of the orbitally excited baryons in the SU(6) **70**-plet [9,10]. In the Hartree language, these are states with $N_c - 1$ quarks in the ground state of the Hartree potential, and one quark in an orbitally excited state. In contrast with the early work done on this problem, our large-N_c arguments lead us to select a very specific set of pion-baryon interactions. Furthermore, there is an important difference between these couplings and those discussed by Dashen, Jenkins, and Manohar for the **56**. In that case, the leading contribution in large N_c is identical to the NRQM prediction (this is related to the fact that the matrix element of the axial vector current is proportional to N_c). However, the dominant decays of the **70** involve the coupling of pions between the **70** and the **56**. These matrix elements do not grow with N_c. The leading large-N_c result then includes additional terms beyond those suggested by the NRQM. Thus we can use our analysis as a test to distinguish between the NRQM and large N_c. This was one of the motivations of the current work. We hoped to see evidence that the additional terms included in the large-N_c analysis were necessary to get an adequate description of the decays. This would have been strong evidence that large N_c has something to do with the success of the NRQM. What we found instead is that the extra terms are not necessary. This result is inconclusive, in the sense that the coefficients of these terms could be small even if the large-N_c counting is correct. But the analysis suggests that there may be more to the NRQM than large N_c.

In the next section, we review the **56** and **70** SU(6) representations of the baryons, as well as their analogs for large N_c. We identify the crucial fact that leads to additional terms in the large-N_c analysis (the mathematical details are reserved for Appendix A). In Sec. III, we discuss our formalism in more detail and present the set of leading operators. In Sec. IV we describe our best fit to the $l = 1$ baryon decays. In Sec. V we present our conclusions. The technical details of our fits to the known s-wave and d-wave decay widths are presented in Appendix B. In Appendix C, we make predictions for the decay modes that have not yet been observed and for the modes that have not been measured precisely.

II. PRELIMINARIES

In this section, we will review the basic elements from Ref. [6] that we later use to fit the decays of the $l = 1$ baryons. A more detailed discussion of these ideas will appear in the next section.

We assume that we can describe the large-N_c baryon states in a tensor product space of the spin-flavor indices of the N_c valence quarks, as in the NRQM. Thus our baryons have the spin-flavor and angular momentum structure of representations of nonrelativistic SU(6)×O(3). We emphasize that we are not assuming SU(6)×O(3). We are not even trying to make sense of this as a symmetry group. Rather, we believe that the assumption follows from a much milder smoothness hy-

pothesis. The argument goes as follows. If the quarks are very heavy compared to Λ_{QCD}, the assumption is clearly correct, because the NRQM description of the baryons can be derived directly from QCD. The splittings between different spin-flavor states with the same spatial wave functions vanish as the quark masses get large. Thus the states break up into approximately degenerate multiplets for each spatial wave function. The different spatial wave functions correspond to different SU(6)×O(3) representations. For example, the ground-state wave function is the completely symmetric spin-flavor combination, corresponding to the Young tableaux shown in Fig. 1, with no orbital angular momentum. The wave functions describing the first excited $l = 1$ baryons correspond to the Young tableaux shown in Fig. 2, symmetrically combined with one unit of orbital angular momentum.

The question is, what happens to these approximately degenerate multiplets as the quarks become light? The thing to notice is that at the bottom of each multiplet (i.e., for states with small total spin), the splittings between neighboring states are not only suppressed by powers of $1/m_q$, but also by powers of $1/N_c$. Thus, barring some phase transition that leads to a discontinuous change in the nature of the baryon states, we expect the bottom of each spin-flavor multiplet to be well described in the same tensor product space that works at large m_q. In other words, the NRQM states should be appropriate.

This argument breaks down at the top of the spin-flavor multiplets, where the baryon spin is of order N_c and the splittings between neighboring spin states are of order Λ_{QCD} for small quark mass. Thus we expect a partial spin-flavor symmetry to survive for small quark mass in large N_c. It is not an approximate symmetry in the usual sense, because symmetry-breaking effects cannot be ignored on any multiplet. Nevertheless, because the dimensions of the multiplets go to infinity as the small parameter $(1/N_c)$ that characterizes the symmetry breaking goes to zero, we can derive reliable predictions at one end (for small spin) of the multiplets even though the symmetry is badly broken at the other. In particular, this argument justifies the use of the NRQM tensor product states to describe the low-spin baryon states for large N_c.

While the argument above is theoretically interesting, it leads to one of the many ambiguities in applying large-N_c arguments to $N_c = 3$. How do we identify states near the "top" and "bottom" of the multiplets for $N_c = 3$? We will ignore this potential difficulty below and use the expressions we derive for the entire baryon multiplets. But we should not be surprised if our results become less reliable as the baryon spin increases.

NRQM versus large N_c. Let us now review in more detail the proposal of Ref. [6] for counting powers of N_c. We will do this for matrix elements of operators between
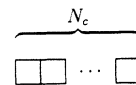
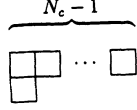FIG. 1. Young tableaux for the spin-flavor representation of the ground-state baryons for large N_c.

$$\overbrace{\qquad\qquad}^{N_c-1}$$

FIG. 2. Young tableaux for the spin-flavor representation of the first excited $l=1$ baryons for large N_c.

baryon states (the operators could be interpolating fields for mesons), ignoring flavor symmetry breaking for simplicity. The procedure is simple: (1) In the spin-flavor space of the NRQM for the baryon states of interest, write down the most general flavor-conserving expression for the matrix element; (2) assign each term in the expression a power of N_c given by the largest possible power that can appear *on the low-spin states*. This is most conveniently determined by simply looking at Feynman diagrams contributing to the matrix element, making appropriate assumptions about the N_c dependence of individual quark matrix elements.

Among the Feynman graphs that contribute to the matrix element is a sum over all quarks of single-quark matrix elements. This has the spin-flavor structure of the NRQM. In all examples we know of, this gives a contribution to the leading N_c dependence. The reason that the suggestion above is nontrivial is that while multiquark diagrams are suppressed by powers of $1/N_c$, their effects can be enhanced by coherent contributions from the sum over the N_c quarks. This can give additional contributions of the same order in N_c as the NRQM but with a different spin-flavor structure.

The possible different spin-flavor structures on quark lines can be divided into four classes.

(1) Constant terms—these always sum coherently over the quarks, but the result has no spin-flavor structure and therefore is not interesting.

(2) Spin terms—these are proportional to

$$\sum_{\text{quarks } x} \sigma_x^j. \tag{2.1}$$

This never adds coherently on low spin states, so these contributions are down by $1/N_c$.

(3) Flavor terms—these are proportional to

$$\sum_{\text{quarks } x} \lambda_x^a. \tag{2.2}$$

This sometimes adds coherently, for example

$$\sum_{\text{quarks } x} \lambda_x^8 \tag{2.3}$$

acting on a low-spin state of u and d quarks is $N_c/\sqrt{12}$.

(4) Spin-flavor terms—these are proportional to

$$\sum_{\text{quarks } x} \sigma_x^j \lambda_x^a. \tag{2.4}$$

This can also add coherently; in fact, we show in Appendix A that the SU(6) quadratic Casimir operator,

$$C_2 \equiv \left[\frac{1}{2f} \sum_j \left(\sum_{\text{quarks } x} \sigma_x^j \right)^2 + \frac{1}{4} \sum_a \left(\sum_{\text{quarks } x} \lambda_x^a \right)^2 \right.$$
$$\left. + \frac{1}{4} \sum_{j,a} \left(\sum_{\text{quarks } x} \sigma_x^j \lambda_x^a \right)^2 \right]$$
$$= \frac{2f-1}{2f} N_c^2 [1 + O(1/N_c)], \tag{2.5}$$

on any finitely excited large-N_c baryon state, where f is the number of flavors. Thus, generically, some spin-flavor matrix elements grow like N_c.

As an example of a one-quark contribution, consider the couplings of the vector mesons, ρ and ω, to the nucleon states. Both couplings grow with N_c, but they are dominated by different contributions. The contribution to the ω matrix element is the flavor coupling (in relativistic notation),

$$\omega_\mu \bar{N} \left(\sum_x \lambda_x^8 \right) \gamma^\mu N, \tag{2.6}$$

while the leading contribution to the ρ coupling is the spin-flavor coupling,

$$(\partial_\mu \rho_\nu^a - \partial_\nu \rho_\mu^a) \bar{N} \left(\sum_x \sigma_x^{\mu\nu} \lambda_x^a \right) N. \tag{2.7}$$

The spin-flavor coupling dominates for the ρ coupling because the isospin matrix element is small for low-spin states, and thus the flavor coupling does not grow with N_c. This is an example of what, in the Skyrme literature, is called the $I_t = J_t$ rule [5,11]. Examples in which multiquark operators contribute at leading order in N_c will appear in the next section.

III. FORMALISM

We are interested in studying the one-pion decays of 70-plet baryons to baryons in the **56**. While there are also **70** → **70** decays, we will not consider them in this paper. The decays to states in the **56** are generally favored by the kinematics, and indeed few **70** → **70** modes have been observed in experiment. In the Hartree language, the part of the interaction Hamiltonian that is of interest to us can be written

$$H = \sum_{n=1}^{N_c} \sum_{\{x_1,\dots,x_n\}\subset\{1,\dots,N_c\}} \int d^3 r_{x_1} \times \cdots \times d^3 r_{x_n} \Phi(r_{x_1})_{x_1}^\dagger \otimes \cdots \otimes \Phi(r_{x_n})_{x_n}^\dagger \mathcal{O}(r_{x_1},\dots,r_{x_n}) \Psi(r_{x_1})_{x_1}$$
$$\otimes \cdots \otimes \Psi(r_{x_{n-1}})_{x_{n-1}} \otimes \Psi_*(r_{x_n})_{x_n}, \tag{3.1}$$

where $\mathcal{O}$ is the pion coupling to the axial-vector quark current.

Equation (3.1) requires some explanation. The Φ's and Ψ's are the individual quark wave functions (the self-consistent solutions to the Hartree equation) for the **56** and **70** baryons, respectively. The sum over n indicates that we have broken up the interaction into parts involving different numbers of quark lines; the second sum accounts for the possible quark interactions with fixed n that connect the initial to the final baryon state. This separation allows us to classify interactions by their order in the $1/N_c$ expansion. By Witten's counting arguments, a general n-body interaction is of order $1/N_c^{n-1}$. For example, there is a distinct term in (3.1) for the $O(1/N_c^2)$ interaction involving three quark lines shown in Fig. 3. In the **70** state, one of the quarks is orbitally excited, which we indicate by the asterisk next to the x_n^{th} quark wave function. Notice that each term in (3.1) involves the wave function Ψ_*, regardless of the number of quark lines involved. This follows because we are only interested in interactions that contribute to the **70** $\to$ **56** decays, which necessarily involve the "deexcitation" of the orbitally excited quark.

While it is much too difficult for us to compute the Hartree potential in a baryon composed of light quarks, we still can learn a great deal by studying the symmetry structure of (3.1). As we argued earlier, it is plausible to represent the small-spin baryon states made from light quarks in the same space, and by the same representations, as the baryon states of the naive quark model. Thus, we work in a $(2f)^{N_c}$-dimensional tensor product space, where f is the number of quark flavors (f is taken as 3 in the fits described in the following section). The quark wave functions Φ and Ψ can be thought of as $2f \times 2f$ matrices acting on the spin-flavor space of a single quark; H as a whole can be thought of as a $(2f)^{N_c} \times (2f)^{N_c}$ matrix acting on the $(2f)^{N_c}$-dimensional spin-flavor space in which we represent the baryon states. The Φ and Ψ are the solutions to the zeroth order Hartree equation, and therefore are spherically symmetric and spin-flavor independent.

Thus, we can replace these matrix wave functions by c numbers

$$\Phi(\mathbf{r}) \to \phi(r), \quad \Psi(\mathbf{r}) \to \psi(r) = \phi(r), \qquad (3.2)$$

where $r = |\mathbf{r}|$. Note that the Hartree potential is a collective phenomenon and to leading order is unaffected by the excitation of a single quark. This accounts for the equality shown in (3.2). In the **70** state, the excited
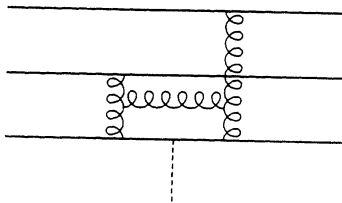

FIG. 3. Feynman graph for a multiquark operator contributing to the pion-baryon coupling in large N_c.

quark has one unit of orbital angular momentum, so we know the form of its spatial wave function:

$$\Psi_*(\mathbf{r}) = f(r)Y_{l=1,m}(\theta, \varphi) = f(r)(\mathbf{r} \cdot \boldsymbol{\varepsilon}_m), \qquad (3.3)$$

where $f(r)$ is a spin-flavor-independent c number. In (3.3) we have chosen to express the $l = 1$ spherical harmonics in terms of the vectors $\boldsymbol{\varepsilon}_m$, which are given by

$$\varepsilon_1 = \frac{1}{\sqrt{2}} \begin{pmatrix} -1 \\ -i \\ 0 \end{pmatrix}, \quad \varepsilon_0 = \begin{pmatrix} 0 \\ 0 \\ 1 \end{pmatrix}, \quad \varepsilon_{-1} = \frac{1}{\sqrt{2}} \begin{pmatrix} 1 \\ -i \\ 0 \end{pmatrix}. \qquad (3.4)$$

Thus, (3.1) is the integral of the operator $\mathcal{O}$ times the product of $2N_c$ spherically symmetric functions times $\mathbf{r} \cdot \boldsymbol{\varepsilon}_m$.

We can formally perform the integrals once we have specified the symmetry structure of the operator $\mathcal{O}$. In the more familiar relativistic notation, the pion-quark coupling is given by

$$(\bar{q}\gamma^\mu\gamma^5\lambda^a q)\partial_\mu\pi^a/f_\pi, \qquad (3.5)$$

where the λ^a are SU(3) generators. In the Hartree basis, the piece of the pion-quark coupling that contributes to baryon decays in the s-wave has the form

$$\mathcal{O} \sim \lambda^a(\boldsymbol{\sigma} \cdot \mathbf{r})\partial^0\pi^a/f_\pi, \qquad (3.6)$$

which, after integration, gives us a one-body interaction that is leading in $1/N_c$:

$$a\lambda_*^a(\boldsymbol{\sigma}_* \cdot \boldsymbol{\varepsilon}_m)\partial^0\pi^a/f_\pi, \qquad (3.7)$$

where a is an unknown coefficient. The asterisk subscript to the spin and flavor matrices indicates that each acts only in the subspace of the orbitally excited quark. Recall that a purely one-body interaction must act on the excited quark line, or there would be no way to change its orbital angular momentum. The spin-flavor structure of the operator in (3.7) is consistent with the predictions of the NRQM. Note that even though one cannot derive (3.7) from (3.5) directly, we know that the nonrelativistic operator must have this form based on the symmetry properties of (3.5). In this sense, the form (3.7) indeed follows from QCD, assuming that the Hartree picture of the baryon is valid.

We can also write down a number of operators that are subleading in $1/N_c$ that involve two quark lines. However, we will only include two of these in our subsequent numerical analysis:

$$ib(\boldsymbol{\sigma}_* \times \boldsymbol{\varepsilon}_m) \cdot \left(\sum_{x\neq*}\lambda_x^a\sigma_x\right)\partial^0\pi^a/f_\pi \qquad (3.8)$$

and

$$c\left(\sum_{x\neq*}\lambda_x^a\right)(\boldsymbol{\sigma}_* \cdot \boldsymbol{\varepsilon}_m)\partial^0\pi^a/f_\pi. \qquad (3.9)$$

Our motivation for retaining these operators is that the sum over $\lambda^a\sigma$ in the case of (3.8) and the sum over λ^a

in the case of (3.9) can both be coherent on low-spin states, and thus the matrix elements can be of order 1, rather than order $1/N_c$. This follows from the argument in Appendix A. Thus we will take our leading s-wave operators to be those given in (3.7), (3.8), and (3.9), which we will call operators A, B, and C, respectively.

Arguments analogous to those that we have used to arrive at the operators responsible for the s-wave decays can also be used to determine the operators responsible

for decays through the d wave. (Note that the decay channels in which the pion has odd orbital angular momentum are forbidden by parity.) The leading one-body operator is given by

$$ d\lambda_*^a \left(\sigma_*^i \varepsilon_m^j + \sigma_*^j \varepsilon_m^i - \tfrac{2}{3} \delta^{ij} \boldsymbol{\sigma}_* \cdot \boldsymbol{\varepsilon}_m \right) \partial^i \partial^j \pi^a / f_\pi^2 . \quad (3.10) $$

We also have two-body operators in the d-wave channel with the same kind of sum that we encountered in (3.8):

$$ ie \sum_{x \neq *} \left[(\boldsymbol{\sigma}_x \times \boldsymbol{\sigma}_*)^i \varepsilon_m^j \lambda_x^a + (\boldsymbol{\sigma}_x \times \boldsymbol{\sigma}_*)^j \varepsilon_m^i \lambda_x^a - \tfrac{2}{3} (\boldsymbol{\sigma}_x \times \boldsymbol{\sigma}_*) \cdot \boldsymbol{\varepsilon}_m \lambda_x^a \delta^{ij} \right] \partial^i \partial^j \pi^a / f_\pi^2 , \quad (3.11) $$

$$ if \sum_{x \neq *} \left[(\boldsymbol{\sigma}_* \times \boldsymbol{\varepsilon}_m)^i \sigma_x^j \lambda_x^a + (\boldsymbol{\sigma}_* \times \boldsymbol{\varepsilon}_m)^j \sigma_x^i \lambda_x^a - \tfrac{2}{3} (\boldsymbol{\sigma}_* \times \boldsymbol{\varepsilon}_m) \cdot \boldsymbol{\sigma}_x \lambda_x^a \delta^{ij} \right] \partial^i \partial^j \pi^a / f_\pi^2 . \quad (3.12) $$

There is also a third two-body operator involving the cross product $(\boldsymbol{\sigma}_x \times \boldsymbol{\varepsilon}_m)$ which is not linearly independent of the two operators that we show above. Finally, there is a d-wave operator analogous to (3.9):

$$ g \left(\sum_{x \neq *} \lambda_x^a \right) (\sigma_*^i \varepsilon_m^j + \sigma_*^j \varepsilon_m^i - \tfrac{2}{3} \delta^{ij} \boldsymbol{\sigma}_* \cdot \boldsymbol{\varepsilon}_m) \partial^i \partial^j \pi^a / f_\pi^2 . $$

$$ (3.13) $$

Thus, we will retain (3.10), (3.11), (3.12), and (3.13) as our set of leading operators in considering the d-wave decays, and refer to them as operators D, E, F, and G.

All that remains is to evaluate our chosen set of operators between the baryon states, constructed in the $(2f)^{N_c}$-dimensional spin-flavor space. While the **56** wave functions can be represented as completely symmetric, three-index SU(6) tensors, we found it more convenient to use a six-index notation in which the spin and flavor of each quark are labeled separately. To represent the **70** states in the most economical way, we add only two new indices—one which labels the orbital angular momentum state of the excited quark, and another which tells us which quark of the three is orbitally excited. We then check that these spin-flavor-orbital angular momentum representations of the states are eigentensors of J^2, J^z, I^2, I^z, ..., with the desired eigenvalues. To compute matrix elements, we first act on n quark indices in the initial baryon state with the desired n-body operator, and sum over the possible combinations; this is equivalent to summing over the quark lines. We then compute the inner product of the result with the tensor representing the final baryon state. In the next section, we use matrix elements computed in this way to determine the partial widths $\Gamma_i^{(\mathrm{pred})}$, used in our fit of the observed s-wave and d-wave pion decays.

IV. FIT

We must now decide precisely which physical quantities we will fit, and select the corresponding experimental

data. In addition, we must arrive at estimates of both the experimental and theoretical uncertainties. The experimental results we will use are the masses, total decay widths, and branching fractions given by the 1992 Particle Data Group (PDG) [12]. We use the experimentally measured masses, rather than large-N_c predictions, in computing partial decay widths. The masses are affected by large logarithmic corrections proportional to m_π^3/f_π^2, which we would have to include if we were to do the calculation properly. For baryons in the **56**, these one-loop corrections are relatively straightforward to compute, because we know the mass eigenstates. For baryons in the **70**, however, we can determine the mass eigenstates only after including the one-loop corrections. This makes the problem of computing the masses nonlinear and thus, far more difficult. For this reason, the problem of predicting **70**-plet masses in the Hartree picture is best treated separately.

A major problem that we encounter in studying the decay widths is that the errors in the experimentally determined values of amplitudes at resonance are often severely underestimated. As a result, one frequently is presented with two or more mutually inconsistent values for a given decay channel. The PDG's approach is to select a few experimental papers that are considered to be relatively trustworthy, and then to produce an estimated range of values that is consistent with most or all of these results. A consequence of this approach is that the uncertainty in the PDG's estimate of a decay width is generally greater than the error quoted in any of the experimental papers from which the estimate is derived. It seems to us that this procedure is safer than the alternative, which is to select one experimental result for each decay width and then fit our parameters to that number, ignoring conflicting experimental results. Of course, the large uncertainties found in the experimental data place a limit on the precision with which we can extract the underlying parameters.

The values which are generally measured experimentally are the amplitudes at resonance $\sqrt{\Gamma_i \Gamma_e}/\Gamma_{\mathrm{tot}}$, from which one can determine the corresponding branching ratios $\Gamma_i/\Gamma_{\mathrm{tot}}$, provided the elasticity $\Gamma_e/\Gamma_{\mathrm{tot}}$ is known (Γ_e is the partial decay width to the initial state parti-

cles used to produce the resonance). Unfortunately, the PDG usually provides estimates for the branching ratios, but not for the amplitudes at resonance. Therefore, it is the branching ratios which we fit in our analysis. Usually this is not a problem, as the uncertainty in the elasticity is reasonably small. In a few cases, however, the elasticity is not very well known, and the uncertainty propagates to all of the decay fractions for that initial state [the $\Sigma(1750)$ resonance is an example]. For consistency, we do not try to produce estimates of the amplitude in these situations; instead, we fit the decay fractions just as we do elsewhere. Finally, we do not attempt to fit those decay channels for which the PDG does not give an estimate; however, predictions for these decay modes do appear in Appendix C.

As far as estimates of experimental error are concerned, ranges such as 10–20 % are interpreted as $15 \pm 5\%$, upper bounds such as $< 10\%$ are converted into $5 \pm 5\%$, and estimates such as $\approx 0.1\%$ are interpreted as $0.1 \pm 0.1\%$. We adopt this scheme simply as a convention, and not because we believe that any of the probability distributions are actually gaussian, with the associated standard deviations. We have found that the precise choice of scheme for treating the experimental data does not significantly affect our results.

In addition to fitting the known decay fractions, we simultaneously fit the total width for each resonance for which at least one decay channel has been measured. In other words, the quantity we minimize is

$$\chi^2 = \sum_{\text{resonance}} \left[\frac{(\Gamma_{\text{tot}}^{(\text{pred})} - \Gamma_{\text{tot}}^{(\text{expt})})^2}{(\Delta\Gamma_{\text{tot}})^2} + \sum_i \frac{\left(\frac{\Gamma_i^{(\text{pred})}}{\Gamma_{\text{tot}}^{(\text{pred})}} - f_i^{(\text{expt})} \right)^2}{(\Delta f_i)^2} \right] . \tag{4.1}$$

The quantities $\Gamma_{\text{tot}}^{(\text{pred})}$ are free to vary, whereas the partial widths $\Gamma_i^{(\text{pred})}$ are functions of our parameters, namely, the coefficients of the leading $1/N_c$ operators and the mixing angles. The alternative to this procedure is to hold the total width for each resonance constant at some best value, and to fit partial widths rather than decay fractions, combining the uncertainties in the total width and in the decay fraction to obtain an uncertainty in the partial width. The former approach is preferred because any uncertainty in a total width $\Gamma_{\text{tot}}^{(\text{expt})}$ is only included once, no matter how many decay channels are measured for that resonance. As for the data on total widths, we again use the PDG. Just as for the decay fractions, the PDG's estimates for total widths are quoted as ranges. Again, we use the midpoint of the range as our best value, and use half the size of the range as our estimate of the uncertainty.

Another issue to be considered is uncertainty in the masses of some of the 70-plet states. For example, the $N(1700)$ mass range is quoted as 1650–1750 MeV. These uncertainties are more important for d-wave decays than for s-wave decays, because the d-wave kinematic factor is more sensitive to the initial state mass. In either case, decays which occur near threshold are more affected by the precise value of the mass than those which occur far from threshold. For the purpose of fitting the data, we ignore this uncertainty, and simply use the "best" estimate of the mass quoted by the PDG. However, as we will see in Appendix C, this possible source of error must be taken into account in our decay predictions.

Theoretical errors also have to be considered. Sources of these errors include subleading operators in the $1/N_c$ expansion, which we have ignored, as well as flavor SU(3) breaking operators. [The only explicit SU(3) breaking effect that we include is the difference between f_π and f_K. We do not consider any operators that distinguish the s quark from the u and d quarks in the baryon. Doing so

would increase the number of free parameters in the fit, and we believe it would not alter the main conclusion of this paper, namely, the suppression of two-body operators. For similar reasons, we treat the η meson as pure octet, neglecting the expected 20 degree mixing with the η'.] As a rough estimate, we have assumed a 20% theoretical uncertainty for each partial width prediction, and have combined this uncertainty in quadrature with the experimental uncertainty. The primary effect of this addition is that the fit is not completely dominated by a few decays which have been measured extremely well experimentally, in particular, the $\Lambda(1520)$ d-wave decays. For the vast majority of decays, the theoretical error is not very important, but for consistency we have used the same value throughout. The choice of a precise value for the theoretical error does not substantially affect the final results.

Note that the estimates for the different decay fractions of a given resonance are not really independent of each other, even though we treat them as such for the purpose of the fit. At the end, we must check that our predicted values for both measured and unmeasured decay widths, together with measured non 56-pion decay widths, add up to the full width to within the allowed uncertainties. In cases where the non-56-pion decays are poorly known, we must at least ascertain that the predicted 56-pion decay fractions sum to a number less than unity. Further details are discussed in Appendices B and C.

In Table I we show the best fit for the measured decays that go entirely through one partial wave. Other fits, involving different mixing angles but very similar values of the parameters a, b, c, d, e, f, and g, are discussed in Appendix B. The definitions of the mixing angles also appear in Appendix B. The quality of the fits is reasonable (the pure s-wave fit has a $\chi^2 = 4.5$ for 4 degrees of freedom, while the pure d-wave fit has a $\chi^2 = 36.0$ for 15 degrees of freedom). With a few exceptions [notable ones

being the $\Lambda(1520) \to N\bar{K}$ and $\Sigma(1775) \to N\bar{K}$ decays], the predictions are within the range of uncertainty given by the combined experimental and theoretical errors.

The most interesting feature of the fit presented in Table I is the smallness of parameters b and c relative to a and of parameters e, f, and g relative to d. When we perform a fit to the same data, omitting the coherent two-body operators, we obtain a somewhat larger χ^2, but qualitatively the fit is quite similar. For example, the best χ^2 for the s-wave fit with only the one-body A operator is 7.9, which is an increase of 3.4 associated with an increase of 2 in the number of degrees of freedom. The situation is similar for the d-wave fit. Thus, the coefficients of the two-body operators are statistically significant, but only marginally so. The unexpected smallness

TABLE I. Predicted branching fractions, corresponding to the parameter set $a = 0.536$, $b = -0.028$, $c = 0.101$, $d = 0.203$, $e = -0.015$, $f = -0.029$, $g = -0.002$, and the mixing angles $\theta_{N1} = 0.61$, $\theta_{N3} = 3.04$, $\theta_{\Lambda 11} = 1.78$, $\theta_{\Lambda 12} = 2.79$, $\theta_{\Lambda 13} = 1.53$, $\theta_{\Lambda 31} = 0.32$, $\theta_{\Lambda 32} = 0.14$, $\theta_{\Lambda 33} = 2.63$, $\theta_{\Sigma 11} = 2.00$, $\theta_{\Sigma 12} = 1.16$, $\theta_{\Sigma 31} = 2.14$, $\theta_{\Sigma 32} = 0.48$.

Decay	$f_{s\text{ wave}}$	$f_{d\text{ wave}}$	f_{expt}
$N(1520) \to N\pi$		65.5	55.0 ± 12.1
$\to N\eta$		0.07	0.1 ± 0.1
$N(1535) \to N\pi$	52.6		45.0 ± 13.4
$\to N\eta$	30.0		40.0 ± 12.8
$\to \Delta\pi$		0.4	5.0 ± 5.0
$N(1650) \to N\pi$	78.4		70.0 ± 17.2
$\to N\eta$	0.9		1.0 ± 1.0
$\to \Lambda K$	3.2		7.0 ± 7.0
$\to \Delta\pi$		9.0	5.0 ± 5.0
$N(1675) \to N\pi$		38.3	45.0 ± 10.3
$\to N\eta$		2.1	1.0 ± 1.0
$\to \Lambda K$		0.005	0.1 ± 0.1
$\to \Delta\pi$		53.7	55.0 ± 12.1
$N(1700) \to N\pi$		13.2	10.0 ± 5.4
$\to \Lambda K$		0.09	0.2 ± 0.1
$\Delta(1620) \to N\pi$	18.7		25.0 ± 7.1
$\to \Delta\pi$		41.8	50.0 ± 14.1
$\Delta(1700) \to N\pi$		12.0	15.0 ± 5.8
$\Lambda(1520) \to N\bar{K}$		17.9	45.0 ± 9.1
$\to \Sigma\pi$		41.5	42.0 ± 8.5
$\Lambda(1670) \to N\bar{K}$	20.2		20.0 ± 6.4
$\to \Sigma\pi$	40.2		40.0 ± 21.5
$\to \Lambda\eta$	25.1		25.0 ± 11.2
$\Lambda(1690) \to N\bar{K}$		21.7	25.0 ± 7.1
$\to \Sigma\pi$		30.3	30.0 ± 11.7
$\Lambda(1800) \to N\bar{K}$	32.6		32.5 ± 9.9
$\Lambda(1830) \to N\bar{K}$		1.3	6.5 ± 3.7
$\to \Sigma\pi$		83.2	55.0 ± 22.8
$\Sigma(1670) \to N\bar{K}$		4.0	10.0 ± 3.6
$\to \Lambda\pi$		11.6	10.0 ± 6.4
$\to \Sigma\pi$		44.4	45.0 ± 17.5
$\Sigma(1750) \to N\bar{K}$	28.1		25.0 ± 15.8
$\to \Sigma\pi$	4.2		4.0 ± 4.0
$\to \Sigma\eta$	6.5		35.0 ± 21.2
$\Sigma(1775) \to N\bar{K}$		17.3	40.0 ± 8.5
$\to \Lambda\pi$		25.6	17.0 ± 4.5
$\to \Sigma\pi$		3.4	3.5 ± 1.7
$\to \Sigma^*\pi$		6.7	10.0 ± 2.8

of these coefficients will be discussed further in the following section.

V. CONCLUSIONS

We have shown how to compute the leading one-pion decay amplitudes for the orbitally excited, 70-plet baryons in the large-N_c limit. By working in a Hartree approximation, we arrived at a specific set of operators that are responsible for decays through the s-wave and d-wave channels. While the fits we obtained to the current experimental data were not necessarily better than those obtained by others using different methods, our results have the advantage of following more directly from the underlying physics in a well-defined limit of QCD.

A striking feature of our results is the suppression of the two-body operators B, C, E, F, and G. Since these operators are one higher order in the $1/N_c$ expansion than A and D, we expected a relative suppression in their coefficients, compensated by an enhancement in the matrix elements. The interesting point is that this suppression was generally much greater than a factor of $N_c = 3$. The two-body operators that we retained all involved a sum over quark lines which we argued should lead to an enhancement of order N_c. However, the values of b, c, e, f, and g that we obtained in the fits were so small that the matrix elements of the two-body operators are suppressed even when the sums over quark lines are coherent.

One possible conclusion from this result is that there is something more to the success of the NRQM for baryons than large N_c. Perhaps somehow, in spite of the fact that the quarks are not really heavy, they act in the process of $l = 1$ baryon decay as if they were.

ACKNOWLEDGMENTS

APPENDIX A: N_c DEPENDENCE OF SPIN-FLAVOR GENERATORS

In this section we derive (2.5). The Casimir operator can be written

$$C_2 \equiv \sum_\alpha T_\alpha^2, \tag{A1}$$

where the T_α are the SU($2f$) generators, normalized so that

$$\text{tr} T_\alpha T_\beta = \delta_{\alpha\beta} \tag{A2}$$

in the defining, $2f$-dimensional representation. Rather than computing the Casimir operator directly in other representations, R, it is easier to compute the quantity $T(R)$, defined by

$$\text{tr}_R T_\alpha T_\beta = T(R)\delta_{\alpha\beta}. \tag{A3}$$

Then C_2 can be obtained as

$$C_2 = (4f^2 - 1)\frac{T(R)}{D(R)}, \tag{A4}$$

where $D(R)$ is the dimension of the representation R. Thus, for example, in the defining representation, the Casimir operator is

$$C_2 = \frac{4f^2 - 1}{2f}. \tag{A5}$$

The crucial step in obtaining (2.5) is to calculate $T(R)$ for the completely symmetric representation of Fig. 1. Let us call this representation $\{N_c\}$. We will calculate the trace of the square of a generator that is the analog of λ^8 for SU$(2f)$:

$$T_{2f-1} \equiv \frac{1}{\sqrt{2f(2f-1)}}\begin{pmatrix} 1 & 0 & \cdots & 0 \\ 0 & 1 & \cdots & 0 \\ \vdots & \vdots & \ddots & \vdots \\ 0 & 0 & \cdots & 1-2f \end{pmatrix}. \tag{A6}$$

Then we can compute the trace by noting that in $\{N_c\}$, there are

$$\begin{pmatrix} N_c + 2f - k - 2 \\ N_c - k \end{pmatrix} \tag{A7}$$

states with k indices having value $2f$, on each of which the value of T_{2f-1}^2 is

$$\frac{1}{2f(2f-1)}[k(1-2f) + (N_c - k)]^2,$$

thus

$$\begin{aligned} T(\{N_c\}) &= \text{tr}_{\{N_c\}} T_{2f-1}^2 \\ &= \frac{1}{2f(2f-1)}\sum_{k=0}^{N_c}[k(2f-1) - (N_c - k)]^2 \\ &\quad \times \begin{pmatrix} N_c + 2f - k - 2 \\ N_c - k \end{pmatrix}, \\ &= \begin{pmatrix} N_c + 2f \\ N_c - 1 \end{pmatrix}. \end{aligned} \tag{A8}$$

This gives

$$C_2(\{N_c\}) = \frac{2f - 1}{2f}N_c(N_c + 2f), \tag{A9}$$

in agreement with (2.5).

The reason that (2.5) is correct for any finitely excited baryon state is that the order N_c^2 term comes from the horizontal string of boxes in the Young tableaux with

length of order N_c, a feature shared by all the finitely excited large-N_c baryon states. More precisely, note that (A9) implies

$$C_2(\{N_c - l\}) = \frac{2f - 1}{2f}N_c^2 + O(N_c) \tag{A10}$$

for any fixed l as $N_c \to \infty$. Note further that we can determine $T(R)$ for any finitely excited baryon state by starting with the representations, $\{N_c - l\}$, and using the recursion relations

$$\begin{aligned} T(r \otimes R) &= D(r)T(R) + D(R)T(r), \\ T(r \otimes R) &= T(r) + T(R). \end{aligned} \tag{A11}$$

The point is that the Clebsch-Gordon decomposition in (A11) does not change C_2 to leading order in N_c because $T(\{N_c - l\})$ is higher order in N_c than $D(\{N_c - l\})$. Thus

$$\begin{aligned} \frac{T(r \otimes \{N_c - l\})}{D(r \otimes \{N_c - l\})} &= \frac{D(r)T(\{N_c - l\}) + D(\{N_c - l\})T(r)}{D(r)D(\{N_c - l\})} \\ &= \frac{T(\{N_c - l\})}{D(\{N_c - l\})} + \text{const} \end{aligned} \tag{A12}$$

for any fixed r. Then the standard rules of Clebsch-Gordon decomposition can be used to establish (2.5) for any representation obtained from $\{N_c - l\}$ by adding a finite number of boxes.

APPENDIX B: FITS OF KNOWN DECAY DATA

1. s-wave decays

We first consider decay channels that are pure s wave, that is, where both the **70** and **56** baryon states have spin-$\frac{1}{2}$. Thirteen such decays have been measured, associated with six **70**-plet resonances. The data is presented in Tables II–IV. The $\Lambda(1405) \to \Sigma\pi$ decay has been

TABLE II. s-wave decays for Δ and N initial states.

	$\Gamma_{tot}^{(expt)}$ (MeV)	$\Gamma_{tot}^{(pred)}$ (MeV)
$\Delta(1620)$	150 ± 30	134.2
	$f_i^{(expt)}$ (%)	$f_i^{(pred)}$ (%)
$\to N\pi$	25.0 ± 7.1	18.7
	$\Gamma_{tot}^{(expt)}$ (MeV)	$\Gamma_{tot}^{(pred)}$ (MeV)
$N(1535)$	175 ± 75	186.5
	$f_i^{(expt)}$ (%)	$f_i^{(pred)}$ (%)
$\to N\pi$	45.0 ± 13.4	52.6
$\to N\eta$	40.0 ± 12.8	30.0
	$\Gamma_{tot}^{(expt)}$ (MeV)	$\Gamma_{tot}^{(pred)}$ (MeV)
$N(1650)$	167.5 ± 22.5	173.1
	$f_i^{(expt)}$ (%)	$f_i^{(pred)}$ (%)
$\to N\pi$	70.0 ± 17.2	78.4
$\to N\eta$	1.0 ± 1.0	0.9
$\to \Lambda K$	7.0 ± 7.1	3.2

TABLE III. s-wave decays for Λ initial states.

		Fit No. 1,6	Fit No. 2,4	Fit No. 3,5	Fit No. 7,8
	$\Gamma_{tot}^{(expt)}$ (MeV)		$\Gamma_{tot}^{(pred)}$ (MeV)		
$\Lambda(1670)$	37.5 ± 12.5	38.1	38.0	32.3	31.5
	$f_i^{(expt)}$ (%)		$f_i^{(pred)}$ (%)		
$\to N\bar{K}$	20.0 ± 6.4	20.2	19.9	20.1	19.1
$\to \Sigma\pi$	40.0 ± 21.5	40.2	39.3	37.1	40.1
$\to \Lambda\eta$	25.0 ± 11.2	25.1	26.1	19.2	20.1
	$\Gamma_{tot}^{(expt)}$ (MeV)		$\Gamma_{tot}^{(pred)}$ (MeV)		
$\Lambda(1800)$	300 ± 100	300.7	300.6	299.0	299.7
	$f_i^{(expt)}$ (%)		$f_i^{(pred)}$ (%)		
$\to N\bar{K}$	32.5 ± 9.9	32.6	32.6	32.4	32.5

omitted from the fit because it is questionable whether the $\Lambda(1405)$ can be described in the SU(6) model. In particular, one suspects that the $\Lambda(1405)$ may consist largely of an unstable $N\bar{K}$ bound state [13]. Our prediction for the $\Lambda(1405) \to \Sigma\pi$ decay rate, 0–10 MeV, based on the assumption that the $\Lambda(1405)$ is an SU(6) state orthogonal to $\Lambda(1670)$ and $\Lambda(1800)$, is in fact much smaller than the measured value, 50 MeV.

Our conventions for the mixing angles are as follows. One angle (θ_{N1}) is needed to specify the spin-$\frac{1}{2}$ nucleon

states:

$$\begin{bmatrix} N(1535) \\ N(1650) \end{bmatrix} = \begin{bmatrix} \cos(\theta_{N1}) & \sin(\theta_{N1}) \\ -\sin(\theta_{N1}) & \cos(\theta_{N1}) \end{bmatrix} \begin{bmatrix} N_{11} \\ N_{31} \end{bmatrix}, \quad (B1)$$

where our convention for the pure SU(6) states on the right-hand side is that the first subscript is twice the total quark spin of the baryon state, and the second is twice the total angular momentum. Three angles ($\theta_{\Lambda 1 i}, i = 1, \ldots, 3$) are used for the Λ mixing matrix:

$$\begin{bmatrix} \Lambda(1670) \\ \Lambda(1800) \\ \Lambda(1405) \end{bmatrix} = \begin{bmatrix} c_{\Lambda 11} c_{\Lambda 12} & s_{\Lambda 11} c_{\Lambda 12} & s_{\Lambda 12} \\ -s_{\Lambda 11} c_{\Lambda 13} - c_{\Lambda 11} s_{\Lambda 13} s_{\Lambda 12} & c_{\Lambda 11} c_{\Lambda 13} - s_{\Lambda 11} s_{\Lambda 13} s_{\Lambda 12} & s_{\Lambda 13} c_{\Lambda 12} \\ s_{\Lambda 11} s_{\Lambda 13} - c_{\Lambda 11} c_{\Lambda 13} s_{\Lambda 12} & -c_{\Lambda 11} s_{\Lambda 13} - s_{\Lambda 11} c_{\Lambda 13} s_{\Lambda 12} & c_{\Lambda 13} c_{\Lambda 12} \end{bmatrix} \begin{bmatrix} \Lambda_{11} \\ \Lambda_{31} \\ \text{Singlet}_{11} \end{bmatrix} \quad (B2)$$

where we use the abbreviation $c_{\Lambda 11} = \cos(\theta_{\Lambda 11})$, etc. Finally, because we have decay data for only one of the three spin-$\frac{1}{2}$ Σ states, only two mixing angles ($\theta_{\Sigma 11}$ and $\theta_{\Sigma 12}$) are needed:

$$\Sigma(1750) = [c_{\Sigma 11} c_{\Sigma 12} \quad s_{\Sigma 11} c_{\Sigma 12} \quad s_{\Sigma 12}] \begin{bmatrix} \Sigma_{11} \\ \Sigma_{31} \\ \Sigma_{11}^* \end{bmatrix}. \quad (B3)$$

Our conventions for all of the mixing matrices and angles are such that if the PDG assignments of the 70-plet states in the quark model were correct, all the mixing matrices would be diagonal and all of the angles would equal 0 (in our fit, we have in fact chosen all of the angles to lie in the interval $[0, \pi)$).

As discussed in Sec. III, we expect three operators A, B, and C to contribute to s-wave decays at leading order in the $1/N_c$ expansion. Thus, we must fit a total of nine parameters (the three coefficients a, b, and c in addition to the six mixing angles) to thirteen decay fractions, leaving us with four degrees of freedom. The best fit produces a χ^2 of 4.47. However, there are a number of minima with χ^2 close to its minimum value, which all have roughly the same values for the parameters a, b, and c, but have different values for the various mixing angles. We found only one solution for the nucleon mixing angle θ_{N1}, eight possible solutions for the Λ mixing matrix, and four solutions for the Σ mixing matrix. All of the

solutions are tabulated in Table V. The quantity $\Delta\chi^2$ associated with each solution is computed relative to our best solution, which has $\chi^2 = 4.47$. For example, if we choose fit No. 3 for the Λ angles and fit No. 4 for the Σ angles, we obtain a total χ^2 of 5.22. Table V also lists the uncertainties in all of the parameters, as obtained from the covariance matrix. The calculated values of the decay fractions corresponding to each of the solutions are listed in Tables II–IV for comparison with experimental data. We present in Tables VI–VIII the spin-$\frac{1}{2}$ N, Λ, and Σ mixing matrices corresponding to the various solutions, along with associated uncertainties.

We note from Table V that the coefficient b is strongly suppressed relative to a, more than one might expect from naive $1/N_c$ power counting, with $N_c = 3$. Because of the uncertainty in the value of c obtained from the fit,

TABLE IV. s-wave decays for Σ initial states.

		Fit No. 1,2	Fit No. 3,4
	$\Gamma_{tot}^{(expt)}$ (MeV)	$\Gamma_{tot}^{(pred)}$ (MeV)	
$\Sigma(1750)$	110 ± 50	109.7	110.1
	$f_i^{(expt)}$ (%)	$f_i^{(pred)}$ (%)	
$\to N\bar{K}$	25.0 ± 15.8	28.1	27.3
$\to \Sigma\pi$	4.0 ± 4.1	4.2	3.8
$\to \Sigma\eta$	35.0 ± 21.2	6.5	2.7

TABLE V. Parameters from s-wave fit.

Parameter	Value
a	0.536 ± 0.071
b	-0.028 ± 0.022
c	0.101 ± 0.059
θ_{N1}	0.61 ± 0.09

	Fit No. 1	Fit No. 2	Fit No. 3	Fit No. 4
$\theta_{\Lambda 11}$	1.78 ± 0.15	1.33 ± 0.19	0.99 ± 0.18	1.33 ± 0.19
$\theta_{\Lambda 12}$	2.79 ± 0.10	2.19 ± 0.15	2.41 ± 0.15	2.19 ± 0.15
$\theta_{\Lambda 13}$	1.53 ± 0.20	1.70 ± 0.19	1.96 ± 0.20	2.71 ± 0.22
$\Delta\chi^2$	0.00	0.01	0.25	0.01

	Fit No. 5	Fit No. 6	Fit No. 7	Fit No. 8
$\theta_{\Lambda 11}$	0.99 ± 0.18	1.78 ± 0.15	1.46 ± 0.15	1.46 ± 0.15
$\theta_{\Lambda 12}$	2.41 ± 0.15	2.79 ± 0.10	2.88 ± 0.10	2.88 ± 0.10
$\theta_{\Lambda 13}$	2.97 ± 0.21	2.54 ± 0.22	2.64 ± 0.21	1.63 ± 0.20
$\Delta\chi^2$	0.25	0.00	0.27	0.27

	Fit No. 1	Fit No. 2	Fit No. 3	Fit No. 4
$\theta_{\Sigma 11}$	2.00 ± 0.29	2.18 ± 0.10	0.77 ± 0.91	1.97 ± 0.14
$\theta_{\Sigma 12}$	1.16 ± 0.47	3.01 ± 0.47	1.29 ± 0.12	2.65 ± 0.31
$\Delta\chi^2$	0.00	0.00	0.50	0.50

it is not as clear that c is strongly suppressed. However, consideration of $s + d$-wave decays in Appendix C leads us to believe that c is in fact near the lower end of the range presented in Table V. For the fitted value of θ_{N1}, we see that there is significant mixing between the N_{11} and N_{31} states. It is somewhat difficult to draw conclusions about the mixing of the Λ and Σ resonances, due to the presence of multiple solutions. For example, fits No. 1 and No. 8 for the Λ angles predict little mixing, but with assignments for the three states different from those given by the PDG. Fits No. 6 and No. 7 also predict a limited amount of mixing, but with the identification of $\Lambda(1800)$ and $\Lambda(1405)$ reversed. Fits Nos. 3–5 all predict a substantial amount of mixing. As far as the Σ states, it is not possible to say definitively whether the $\Sigma(1750)$ consists mostly of Σ_{31} or of Σ_{11}^*.

In Table III, we see that the most obvious difference between fits Nos. 1, 2, 4, 6 and fits Nos. 3, 5, 7, 8 is that the latter predict a smaller partial width for $\Lambda(1670) \rightarrow \Lambda\eta$. In Table IV, we notice that the main problem with $\Sigma(1750)$ decays is to obtain a reasonable value for the $\Sigma\eta$ channel.

2. d-wave decays

The same procedure is followed as for the s-wave decay rates. Here, we only fit those decays which are pure d-wave, that is, we omit spin-$\frac{3}{2}$ to spin-$\frac{3}{2}$ decays (these will be discussed in Appendix C). Our conventions for the mixing angles of the spin-$\frac{3}{2}$ states are analogous to those for the spin-$\frac{1}{2}$ states. For the nucleons,

TABLE VI. Spin-$\frac{1}{2}$ nucleon mixing matrix.

$$M_{N1} = \begin{bmatrix} 0.82 \pm 0.05 & 0.57 \pm 0.07 \\ -0.57 \pm 0.07 & 0.82 \pm 0.05 \end{bmatrix}$$

$$\begin{bmatrix} N(1520) \\ N(1700) \end{bmatrix} = \begin{bmatrix} \cos(\theta_{N3}) & \sin(\theta_{N3}) \\ -\sin(\theta_{N3}) & \cos(\theta_{N3}) \end{bmatrix} \begin{bmatrix} N_{13} \\ N_{33} \end{bmatrix}. \quad \text{(B4)}$$

For the Λ states,

TABLE VII. Spin-$\frac{1}{2}$ Λ mixing matrices.

$$M_{\Lambda 1}^{(\text{fit No. 1})} = \begin{bmatrix} 0.19 \pm 0.14 & -0.92 \pm 0.04 & 0.34 \pm 0.09 \\ 0.03 \pm 0.19 & -0.35 \pm 0.11 & -0.94 \pm 0.04 \\ 0.98 \pm 0.03 & 0.19 \pm 0.16 & -0.04 \pm 0.19 \end{bmatrix}$$

$$M_{\Lambda 1}^{(\text{fit No. 2})} = \begin{bmatrix} -0.14 \pm 0.12 & -0.56 \pm 0.11 & 0.81 \pm 0.09 \\ -0.07 \pm 0.20 & -0.81 \pm 0.08 & -0.58 \pm 0.12 \\ 0.99 \pm 0.03 & -0.13 \pm 0.20 & 0.07 \pm 0.12 \end{bmatrix}$$

$$M_{\Lambda 1}^{(\text{fit No. 3})} = \begin{bmatrix} -0.41 \pm 0.14 & -0.62 \pm 0.09 & 0.67 \pm 0.11 \\ -0.02 \pm 0.18 & -0.72 \pm 0.10 & -0.69 \pm 0.11 \\ 0.91 \pm 0.06 & -0.30 \pm 0.19 & 0.28 \pm 0.14 \end{bmatrix}$$

$$M_{\Lambda 1}^{(\text{fit No. 4})} = \begin{bmatrix} -0.14 \pm 0.12 & -0.56 \pm 0.11 & 0.81 \pm 0.09 \\ 0.80 \pm 0.09 & -0.55 \pm 0.12 & -0.24 \pm 0.11 \\ 0.58 \pm 0.13 & 0.62 \pm 0.10 & 0.53 \pm 0.14 \end{bmatrix}$$

$$M_{\Lambda 1}^{(\text{fit No. 5})} = \begin{bmatrix} -0.41 \pm 0.14 & -0.62 \pm 0.09 & 0.67 \pm 0.11 \\ 0.76 \pm 0.08 & -0.64 \pm 0.09 & -0.13 \pm 0.15 \\ 0.50 \pm 0.14 & 0.46 \pm 0.12 & 0.73 \pm 0.11 \end{bmatrix}$$

$$M_{\Lambda 1}^{(\text{fit No. 6})} = \begin{bmatrix} 0.19 \pm 0.14 & -0.92 \pm 0.04 & 0.34 \pm 0.09 \\ 0.85 \pm 0.11 & -0.02 \pm 0.14 & -0.53 \pm 0.17 \\ 0.49 \pm 0.16 & 0.40 \pm 0.09 & 0.77 \pm 0.13 \end{bmatrix}$$

$$M_{\Lambda 1}^{(\text{fit No. 7})} = \begin{bmatrix} -0.11 \pm 0.14 & -0.96 \pm 0.03 & 0.26 \pm 0.10 \\ 0.86 \pm 0.09 & -0.22 \pm 0.11 & -0.46 \pm 0.18 \\ 0.50 \pm 0.17 & 0.17 \pm 0.10 & 0.85 \pm 0.11 \end{bmatrix}$$

$$M_{\Lambda 1}^{(\text{fit No. 8})} = \begin{bmatrix} -0.11 \pm 0.14 & -0.96 \pm 0.03 & 0.26 \pm 0.10 \\ 0.03 \pm 0.19 & -0.26 \pm 0.10 & -0.96 \pm 0.03 \\ 1.00 \pm 0.02 & -0.10 \pm 0.14 & 0.06 \pm 0.19 \end{bmatrix}$$

$$\begin{bmatrix} \Lambda(1690) \\ \Lambda(??) \\ \Lambda(1520) \end{bmatrix} = \begin{bmatrix} c_{\Lambda31}c_{\Lambda32} & s_{\Lambda31}c_{\Lambda32} & s_{\Lambda32} \\ -s_{\Lambda31}c_{\Lambda33} - c_{\Lambda31}s_{\Lambda33}s_{\Lambda32} & c_{\Lambda31}c_{\Lambda33} - s_{\Lambda31}s_{\Lambda33}s_{\Lambda32} & s_{\Lambda33}c_{\Lambda32} \\ s_{\Lambda31}s_{\Lambda33} - c_{\Lambda31}c_{\Lambda33}s_{\Lambda32} & -c_{\Lambda31}s_{\Lambda33} - s_{\Lambda31}c_{\Lambda33}s_{\Lambda32} & c_{\Lambda33}c_{\Lambda32} \end{bmatrix} \begin{bmatrix} \Lambda_{13} \\ \Lambda_{33} \\ \text{Singlet}_{13} \end{bmatrix} \qquad (B5)$$

Here $\Lambda(??)$ is the unidentified spin-$\frac{3}{2}$ **70**-plet Λ state, orthogonal to $\Lambda(1690)$ and $\Lambda(1520)$. Although the physical state has not been identified, we can make predictions for its decay widths into the allowed **56**-pion channels, provided that we make a reasonable guess at its mass. Finally, only one of the spin-$\frac{3}{2}$ Σ states has been identified, and we parametrize it as follows:

$$\Sigma(1775) = \begin{bmatrix} c_{\Sigma31}c_{\Sigma32} & s_{\Sigma31}c_{\Sigma32} & s_{\Sigma32} \end{bmatrix} \begin{bmatrix} \Sigma_{13} \\ \Sigma_{33} \\ \Sigma_{13}^* \end{bmatrix}. \qquad (B6)$$

For the spin-$\frac{1}{2}$ nucleon pure d-wave decays (for which only upper bounds are known), we use the mixing angle obtained by fitting the s-wave decays, namely, $\theta_{N1} = 0.61$.

The coefficients of the operators D, E, F, and G, together with the six new mixing angles, combine to give us ten parameters. With 25 decay fractions to be fitted, there are 15 degrees of freedom. The best fit has $\chi^2 = 36.0$. As with the s-wave decays, although the coefficients d, e, f, and g are reasonably constrained by the fitting procedure, there are several solutions for the mixing angles, all of which have a value of χ^2 close to the minimum value. We obtain two solutions for the spin-$\frac{3}{2}$ nucleon mixing matrix, four solutions for spin-$\frac{3}{2}$ Λ mixing, and two solutions for the $\Sigma(1775)$ state. The calculated decay fractions for each set of parameters are presented in Tables IX–XII, together with the corresponding experimental data. All the solutions for the three coefficients and the six mixing angles are tabulated in Table XIII. The corresponding spin-$\frac{3}{2}$ mixing matrices are found in Tables XIV–XVI.

We see from Table XIII that the coefficients e, f, and g are strongly suppressed relative to d, which is consistent with what we found for the s-wave decays. Comparing predicted and experimental branching fractions, we see that a large part of the total χ^2 comes from the $\Lambda(1520) \to N\bar{K}$ decay. $\Sigma(1775) \to N\bar{K}$ also seems strongly enhanced relative to our predictions.

TABLE VIII. Spin-$\frac{1}{2}$ Σ mixing matrices.

$M_{\Sigma1}^{(\text{fit No. 1})} = [-0.17 \pm 0.27 \quad 0.36 \pm 0.35 \quad 0.92 \pm 0.19]$

$M_{\Sigma1}^{(\text{fit No. 2})} = [0.57 \pm 0.07 \quad -0.81 \pm 0.09 \quad 0.13 \pm 0.46]$

$M_{\Sigma1}^{(\text{fit No. 3})} = [0.20 \pm 0.15 \quad 0.19 \pm 0.23 \quad 0.96 \pm 0.03]$

$M_{\Sigma1}^{(\text{fit No. 4})} = [0.34 \pm 0.11 \quad -0.81 \pm 0.16 \quad 0.47 \pm 0.27]$

APPENDIX C: DECAY PREDICTIONS

In this appendix we predict the partial widths for all of the remaining kinematically allowed one-pion decays. We display a different set of predictions corresponding to each of the fits presented in Appendix B.

While it was more convenient for us to work with branching fractions in the preceding section, here we

TABLE IX. d-wave decays with no spin-$\frac{3}{2}$ mixing.

$\Delta(1620)$	$\Gamma_{\text{tot}}^{(\text{expt})}$ (MeV)	$\Gamma_{\text{tot}}^{(\text{pred})}$ (MeV)
	150 ± 30	138.8
	$f_i^{(\text{expt})}$ (%)	$f_i^{(\text{pred})}$ (%)
$\to \Delta\pi$	50.0 ± 14.1	41.8

$\Lambda(1700)$	$\Gamma_{\text{tot}}^{(\text{expt})}$ (MeV)	$\Gamma_{\text{tot}}^{(\text{pred})}$ (MeV)
	300 ± 100	259.7
	$f_i^{(\text{expt})}$ (%)	$f_i^{(\text{pred})}$ (%)
$\to N\pi$	15.0 ± 5.8	12.0

$N(1535)$	$\Gamma_{\text{tot}}^{(\text{expt})}$ (MeV)	$\Gamma_{\text{tot}}(\text{pred})$ (MeV)
	175 ± 75	186.5
	$f_i^{(\text{expt})}$ (%)	$f_i^{(\text{pred})}$ (%)
$\to \Delta\pi$	5.0 ± 5.1	0.4

$N(1650)$	$\Gamma_{\text{tot}}^{(\text{expt})}$ (MeV)	$\Gamma_{\text{tot}}^{(\text{pred})}$ (MeV)
	167.5 ± 22.5	173.1
	$f_i^{(\text{expt})}$ (%)	$f_i^{(\text{pred})}$ (%)
$\to \Delta\pi$	5.0 ± 5.1	9.0

$N(1675)$	$\Gamma_{\text{tot}}^{(\text{expt})}$ (MeV)	$\Gamma_{\text{tot}}^{(\text{pred})}$ (MeV)
	160 ± 20	158.0
	$f_i^{(\text{expt})}$ (%)	$f_i^{(\text{pred})}$ (%)
$\to N\pi$	45.0 ± 10.3	38.3
$\to N\eta$	1.0 ± 1.0	2.1
$\to \Lambda K$	0.1 ± 0.1	0.005
$\to \Delta\pi$	55.0 ± 12.1	53.7

$\Lambda(1830)$	$\Gamma_{\text{tot}}^{(\text{expt})}$ (MeV)	$\Gamma_{\text{tot}}^{(\text{pred})}$ (MeV)
	85 ± 25	108.2
	$f_i^{(\text{expt})}$ (%)	$f_i^{(\text{pred})}$ (%)
$\to N\bar{K}$	6.5 ± 3.7	1.3
$\to \Sigma\pi$	55.0 ± 22.8	83.2

$\Sigma(1775)$	$\Gamma_{\text{tot}}^{(\text{expt})}$ (MeV)	$\Gamma_{\text{tot}}^{(\text{pred})}$ (MeV)
	120 ± 15	124.5
	$f_i^{(\text{expt})}$ (%)	$f_i^{(\text{pred})}$ (%)
$\to N\bar{K}$	40.0 ± 8.5	17.3
$\to \Lambda\pi$	17.0 ± 4.5	25.6
$\to \Sigma\pi$	3.5 ± 1.7	3.4
$\to \Sigma^*\pi$	10.0 ± 2.8	6.7

TABLE X. d-wave decays for spin-$\frac{3}{2}$ nucleon initial states.

		Fit No. 1	Fit No. 2
	$\Gamma_{tot}^{(expt)}$ (MeV)	$\Gamma_{tot}^{(pred)}$ (MeV)	
$N(1520)$	122.5 ± 12.5	128.0	128.0
	$f_i^{(expt)}$ (%)	$f_i^{(pred)}$ (%)	
$\rightarrow N\pi$	55.0 ± 12.1	65.5	65.4
$\rightarrow N\eta$	0.1 ± 0.1	0.07	0.08
	$\Gamma_{tot}^{(expt)}$ (MeV)	$\Gamma_{tot}^{(pred)}$ (MeV)	
$N(1700)$	100 ± 50	101.3	107.3
	$f_i^{(expt)}$ (%)	$f_i^{(pred)}$ (%)	
$\rightarrow N\pi$	10.0 ± 5.4	13.2	11.9
$\rightarrow \Lambda K$	0.2 ± 0.1	0.09	0.03

TABLE XI. d-wave decays for spin-$\frac{3}{2}$ Λ initial states.

		Fit No. 1,3	Fit No. 2,4
	$\Gamma_{tot}^{(expt)}$ (MeV)	$\Gamma_{tot}^{(pred)}$ (MeV)	
$\Lambda(1690)$	60 ± 10	57.6	55.2
	$f_i^{(expt)}$ (%)	$f_i^{(pred)}$ (%)	
$\rightarrow N\bar{K}$	25.0 ± 7.1	21.7	20.9
$\rightarrow \Sigma\pi$	30.0 ± 11.7	30.3	24.9
	$\Gamma_{tot}^{(expt)}$ (MeV)	$\Gamma_{tot}^{(pred)}$ (MeV)	
$\Lambda(1520)$	15.6 ± 1.0	15.2	15.1
	$f_i^{(expt)}$ (%)	$f_i^{(pred)}$ (%)	
$\rightarrow N\bar{K}$	45.0 ± 9.1	17.9	14.4
$\rightarrow \Sigma\pi$	42.0 ± 8.5	41.5	36.3

present our results directly in terms of partial widths. The errors we present for these predictions are a combination of the uncertainties in the parameters given in Tables V and XIII, and the uncertainties in the masses of the initial states. The latter have a large effect on our predictions for the decays that are near threshold, due to the momentum dependence of the squared amplitudes. For decays very near threshold, we are able to obtain only an upper bound for the partial width. In Tables XVII–XXII we list the decay predictions, the total decay widths $\Gamma_{tot}^{(pred)}$ given in Appendix B, and the experimentally measured total widths $\Gamma_{tot}^{(expt)}$.

Among our predictions are six decays that can proceed through both the s- and d-wave channels. (We will refer to these as $s + d$-wave decays.) Three of these have been measured reasonably well, while the others are either poorly known or unobserved. We have chosen not to include the former three in our fits in Appendix B, to simplify our analysis. In principle, a proper treatment would require fitting the pure s-wave, the pure d-wave, and the $s + d$-wave decays simultaneously. Instead we simply check in this section that the predictions for the three measured $s+d$-wave decays are in reasonable agreement with the experimental results.

1. Decays involving no mixing angles

We first consider predictions of the partial decay widths that do not involve mixing angles. The unmixed initial states are the spin-$\frac{1}{2}$ $\Delta(1620)$, the spin-$\frac{3}{2}$ $\Delta(1700)$, and the spin-$\frac{5}{2}$ $N(1675)$, $\Lambda(1830)$, and $\Sigma(1775)$. The kinematically allowed decays that we have not already considered in Appendix B are listed in Table XVII. The $\Delta(1700) \rightarrow \Delta\pi$ is one of the $s + d$-wave decays that have been adequately measured. Our prediction of 271 ± 126 MeV is compatible with the PDG's value of $(0.45 \pm 0.1) \times (300 \pm 100)$ MeV if we take the partial width to lie at the lower end of the predicted range. Analysis of the dependence of our prediction on the various parameters suggests that the c parameter should take its value at the bottom of the range given in Table V.

2. Nucleon decays

All the kinematically allowed spin-$\frac{1}{2}$ N decays have been included in Appendix B. Predictions for the spin-$\frac{3}{2}$ nucleons are shown in Table XVIII. The $N(1520) \rightarrow \Delta\pi$ is another of the three known $s + d$-wave decays. The PDG's value $(0.22 \pm 0.08) \times (122 \pm 13)$ MeV for its partial width strongly favors fit No. 1. Furthermore, the PDG's partial wave analysis of this decay is consistent with fit No. 1, but incompatible with fit No. 2. Therefore we conclude that fit No. 1 has the correct mixing angle.

The $N(1700) \rightarrow \Delta\pi$ is the third of the known $s + d$-wave decays. Our fit No. 1 prediction of 180 ± 74 MeV is large compared to the PDG's value of $(0.38 \pm 0.32)(100 \pm 50)$ MeV. However, if we adopt a value of the $N(1700)$ full width that is just within the PDG's upper limit, while also using the smallest prediction for the $N(1700) \rightarrow \Delta\pi$ width consistent with our range of error, we obtain a branching fraction that is in reasonable agreement with experiment. This increase in the total decay width still allows good fits for the $N(1700) \rightarrow N\pi$ and $N(1700) \rightarrow \Lambda K$ decay fractions (see Table X). If we had included the $N(1700) \rightarrow \Delta\pi$ decay in the fits in Appendix B, the only substantial change would have been an increase in the $N(1700)$ predicted full width.

3. Λ decays

There are four allowed spin-$\frac{1}{2}$ Λ decays, listed in Table XIX. The one measurement from the PDG for the

TABLE XII. d-wave decays for spin-$\frac{3}{2}$ Σ initial states.

		Fit No. 1	Fit No. 2
	$\Gamma_{tot}^{(expt)}$ (MeV)	$\Gamma_{tot}^{(pred)}$ (MeV)	
$\Sigma(1670)$	60 ± 20	49.5	7.3
	$f_i^{(expt)}$ (%)	$f_i^{(pred)}$ (%)	
$\rightarrow N\bar{K}$	10.0 ± 3.6	4.0	8.4
$\rightarrow \Lambda\pi$	10.0 ± 6.4	11.6	10.8
$\rightarrow \Sigma\pi$	45.0 ± 17.5	44.4	43.5

TABLE XIII. Parameters from d-wave fit.

Parameter	Value
d	0.203 ± 0.011
e	-0.015 ± 0.004
f	-0.029 ± 0.008
g	-0.002 ± 0.005

	Fit No. 1	Fit No. 2		
θ_{N3}	3.04 ± 0.15	2.60 ± 0.16		
$\Delta\chi^2$	0.00	1.27		

	Fit No. 1	Fit No. 2	Fit No. 3	Fit No. 4
$\theta_{\Lambda 31}$	0.32 ± 0.25	1.04 ± 0.18	2.20 ± 0.25	1.45 ± 0.18
$\theta_{\Lambda 32}$	0.14 ± 0.08	2.61 ± 0.10	2.93 ± 0.07	0.42 ± 0.10
$\theta_{\Lambda 33}$	2.63 ± 0.17	0.45 ± 0.15	0.42 ± 0.17	2.72 ± 0.15
$\Delta\chi^2$	0.00	3.55	0.00	3.55

	Fit No. 1	Fit No. 2
$\theta_{\Sigma 31}$	2.14 ± 0.37	1.00 ± 0.11
$\theta_{\Sigma 32}$	0.48 ± 0.22	0.76 ± 0.34
$\Delta\chi^2$	0.00	4.03

TABLE XIV. Spin-$\frac{3}{2}$ nucleon mixing matrices.

$$M_{N3}^{(\text{fit No. 1})} = \begin{bmatrix} -0.99 \pm 0.02 & 0.10 \pm 0.15 \\ -0.10 \pm 0.15 & -0.99 \pm 0.02 \end{bmatrix}$$

$$M_{N3}^{(\text{fit No. 2})} = \begin{bmatrix} -0.85 \pm 0.08 & 0.52 \pm 0.14 \\ -0.52 \pm 0.14 & -0.85 \pm 0.08 \end{bmatrix}$$

TABLE XV. Spin-$\frac{3}{2}$ Λ mixing matrices.

$$M_{\Lambda 3}^{(\text{fit No. 1})} = \begin{bmatrix} 0.94 \pm 0.07 & 0.31 \pm 0.24 & 0.14 \pm 0.08 \\ 0.20 \pm 0.24 & -0.85 \pm 0.10 & 0.48 \pm 0.15 \\ 0.27 \pm 0.09 & -0.43 \pm 0.15 & -0.86 \pm 0.08 \end{bmatrix}$$

$$M_{\Lambda 3}^{(\text{fit No. 2})} = \begin{bmatrix} -0.44 \pm 0.15 & -0.74 \pm 0.08 & 0.51 \pm 0.09 \\ -0.89 \pm 0.07 & 0.27 \pm 0.18 & -0.37 \pm 0.13 \\ 0.14 \pm 0.16 & -0.61 \pm 0.06 & -0.78 \pm 0.06 \end{bmatrix}$$

$$M_{\Lambda 3}^{(\text{fit No. 3})} = \begin{bmatrix} 0.58 \pm 0.19 & -0.79 \pm 0.15 & 0.21 \pm 0.07 \\ -0.69 \pm 0.15 & -0.61 \pm 0.19 & -0.40 \pm 0.16 \\ 0.44 \pm 0.12 & 0.09 \pm 0.14 & -0.89 \pm 0.06 \end{bmatrix}$$

$$M_{\Lambda 3}^{(\text{fit No. 4})} = \begin{bmatrix} 0.11 \pm 0.16 & 0.91 \pm 0.05 & 0.41 \pm 0.09 \\ 0.89 \pm 0.08 & -0.28 \pm 0.18 & 0.37 \pm 0.13 \\ 0.45 \pm 0.14 & 0.32 \pm 0.11 & -0.83 \pm 0.05 \end{bmatrix}$$

TABLE XVI. Spin-$\frac{3}{2}$ Σ mixing matrices.

$$M_{\Sigma 3}^{(\text{fit No. 1})} = [-0.48 \pm 0.27 \quad 0.75 \pm 0.22 \quad 0.46 \pm 0.19]$$

$$M_{\Sigma 3}^{(\text{fit No. 2})} = [0.39 \pm 0.10 \quad 0.61 \pm 0.23 \quad 0.69 \pm 0.24]$$

TABLE XVII. Predictions involving no mixing angles.

$\Delta(1700)$	$\Gamma_{\text{tot}}^{(\text{expt})}$ (MeV)	$\Gamma_{\text{tot}}^{(\text{pred})}$ (MeV)
	300 ± 100	260
		$\Gamma_i^{(\text{pred})}$ (MeV)
$\rightarrow \Delta\pi$		271 ± 126
s wave		241 ± 117
d wave		30 ± 18
$\rightarrow \Sigma K$		< 0.25

$\Lambda(1830)$	$\Gamma_{\text{tot}}^{(\text{expt})}$ (MeV)	$\Gamma_{\text{tot}}^{(\text{pred})}$ (MeV)
	85 ± 25	108
		$\Gamma_i^{(\text{pred})}$ (MeV)
$\rightarrow \Lambda\eta$		4.9 ± 1.0
$\rightarrow \Xi K$		< 0.01

$\Sigma(1775)$	$\Gamma_{\text{tot}}^{(\text{expt})}$ (MeV)	$\Gamma_{\text{tot}}^{(\text{pred})}$ (MeV)
	120 ± 15	125
		$\Gamma_i^{(\text{pred})}$ (MeV)
$\rightarrow \Sigma\eta$		0.12 ± 0.04
$\rightarrow \Delta\bar{K}$		0.85 ± 0.23

TABLE XVIII. Predictions for decays of spin-$\frac{3}{2}$ N initial states.

		Fit No. 1	Fit No. 2
	$\Gamma_{\text{tot}}^{(\text{expt})}$ (MeV)	$\Gamma_{\text{tot}}^{(\text{pred})}$ (MeV)	
$N(1520)$	122.5 ± 12.5	128.0	128.0
		$\Gamma_i^{(\text{pred})}$ (MeV)	
$\rightarrow \Delta\pi$		18.0 ± 4.4	9.8 ± 1.9
s wave		10.6 ± 3.4	0.03 ± 0.01
d wave		7.5 ± 2.5	9.8 ± 1.9
	$\Gamma_{\text{tot}}^{(\text{expt})}$ (MeV)	$\Gamma_{\text{tot}}^{(\text{pred})}$ (MeV)	
$N(1700)$	100 ± 50	101.3	107.3
		$\Gamma_i^{(\text{pred})}$ (MeV)	
$\rightarrow \Delta\pi$		180 ± 74	189 ± 76
s wave		151 ± 61	188 ± 76
d wave		29 ± 27	< 5
$\rightarrow N\eta$		1.5 ± 1.2	< 0.2
$\rightarrow \Sigma K$		< 0.03	< 0.004

TABLE XIX. Predictions for decays of spin-$\frac{1}{2}$ Λ initial states.

		Fit No. 1	Fit No. 2	Fit No. 3	Fit No. 4
	$\Gamma_{\text{tot}}^{(\text{expt})}$ (MeV)		$\Gamma_{\text{tot}}^{(\text{pred})}$ (MeV)		
$\Lambda(1670)$	37.5 ± 12.5	38.1	38.0	32.3	38.0
			$\Gamma_i^{(\text{pred})}$ (MeV)		
$\rightarrow \Sigma^* \pi$		0.72 ± 0.36	0.034 ± 0.017	< 0.03	0.034 ± 0.017
		Fit No. 5	Fit No. 6	Fit No. 7	Fit No. 8
			$\Gamma_{\text{tot}}^{(\text{pred})}$ (MeV)		
$\Lambda(1670)$		32.3	38.1	31.5	31.5
			$\Gamma_i^{(\text{pred})}$ (MeV)		
$\rightarrow \Sigma^* \pi$		< 0.03	0.72 ± 0.36	0.23 ± 0.11	0.23 ± 0.12
		Fit No. 1	Fit No. 2	Fit No. 3	Fit No. 4
	$\Gamma_{\text{tot}}^{(\text{expt})}$ (MeV)		$\Gamma_{\text{tot}}^{(\text{pred})}$ (MeV)		
$\Lambda(1800)$	300 ± 100	300.7	300.6	299.0	300.6
			$\Gamma_i^{(\text{pred})}$ (MeV)		
$\rightarrow \Sigma \pi$		187 ± 116	170 ± 101	191 ± 109	148 ± 59
$\rightarrow \Sigma^* \pi$		0.53 ± 0.44	1.5 ± 1.2	1.5 ± 1.2	15 ± 12
$\rightarrow \Lambda \eta$		18 ± 14	< 0.25	< 4	15 ± 9
		Fit No. 5	Fit No. 6	Fit No. 7	Fit No. 8
			$\Gamma_{\text{tot}}^{(\text{pred})}$ (MeV)		
$\Lambda(1800)$		299.0	300.7	299.7	299.7
			$\Gamma_i^{(\text{pred})}$ (MeV)		
$\rightarrow \Sigma \pi$		130 ± 59	125 ± 57	149 ± 61	175 ± 122
$\rightarrow \Sigma^* \pi$		15 ± 12	9.3 ± 7.8	12 ± 10	0.33 ± 0.28
$\rightarrow \Lambda \eta$		24 ± 13	< 2	< 4	23 ± 15

TABLE XX. Predictions for decays of spin-$\frac{3}{2}$ Λ initial states.

		Fit No. 1	Fit No. 2	Fit No. 3	Fit No. 4
	$\Gamma_{\text{tot}}^{(\text{expt})}$ (MeV)		$\Gamma_{\text{tot}}^{(\text{pred})}$ (MeV)		
$\Lambda(1690)$	60 ± 10	57.6	55.2	57.6	55.2
			$\Gamma_i^{(\text{pred})}$ (MeV)		
$\rightarrow \Lambda \eta$		< 0.01	< 0.1	< 0.001	< 0.04
$\rightarrow \Sigma^* \pi$		32 ± 10	36 ± 12	15.8 ± 2.9	36 ± 11
s wave		28.5 ± 9.1	36 ± 12	6.3 ± 2.0	33 ± 11
d wave		3.9 ± 3.1	< 0.4	9.5 ± 2.1	2.1 ± 1.8
	$\Gamma_{\text{tot}}^{(\text{expt})}$ (MeV)[a]		$\Gamma_{\text{tot}}^{(\text{pred})}$ (MeV)[a]		
$\Lambda(??)$	$-$	$-$	$-$	$-$	$-$
			$\Gamma_i^{(\text{pred})}$ (MeV)		
$\rightarrow N\bar{K}$		< 3	38 ± 29	< 3	38 ± 29
$\rightarrow \Sigma \pi$		105 ± 69	140 ± 65	105 ± 69	139 ± 65
$\rightarrow \Lambda \eta$		2.6 ± 3.3	< 0.4	< 2.5	< 0.4
$\rightarrow \Sigma^* \pi$		97 ± 46	85 ± 43	120 ± 49	85 ± 43
s wave		55 ± 22	9.3 ± 3.7	116 ± 47	8.6 ± 3.5
d wave		42 ± 32	75 ± 41	< 15	76 ± 41

[a]Unknown.

TABLE XXI. Predictions for decays of spin-$\frac{1}{2}$ Σ initial states.

		Fit No. 1	Fit No. 2	Fit No. 3	Fit No. 4
	$\Gamma_{\text{tot}}^{(\text{expt})}$ (MeV)		$\Gamma_{\text{tot}}^{(\text{pred})}$ (MeV)		
$\Sigma(1750)$	110 ± 50	109.7	109.7	110.1	110.1
			$\Gamma_i^{(\text{pred})}$ (MeV)		
$\rightarrow \Lambda \pi$		< 7	43 ± 22	< 20	49 ± 12
$\rightarrow \Sigma^* \pi$		25 ± 17	< 0.7	22 ± 15	2.1 ± 1.6
$\rightarrow \Delta\bar{K}$		< 1.4	< 0.9	< 2.5	< 1.7

TABLE XXII. Predictions for decays of spin-$\frac{3}{2}$ Σ initial states.

	$\Gamma_{tot}^{(expt)}$ (MeV)	Fit No. 1 $\Gamma_{tot}^{(pred)}$ (MeV)	Fit No. 2
$\Sigma(1670)$	60 ± 20	49.5	7.3
		$\Gamma_i^{(pred)}$ (MeV)	
$\to \Sigma^* \pi$		15.8 ± 4.8	41 ± 12
s wave		15.5 ± 4.6	40 ± 12
d wave		0.27 ± 0.35	0.57 ± 0.61

$\Lambda(1670) \to \Sigma^* \pi$ width, 6 ± 3 MeV, is somewhat larger than our predictions, and favors fits No. 1 and No. 6. Of the six spin-$\frac{3}{2}$ Λ decays shown in Table XX, four involve the unobserved Λ state which is orthogonal to the $\Lambda(1520)$ and $\Lambda(1690)$. To compute the decay widths of the unobserved state, we made a reasonable guess at its mass based on the nucleon-Λ splitting found in other multiplets. The mass we adopted was 1850 ± 50 MeV. The

four widths involving the unobserved state have large errors in part because there are no known decays to fit the mixing angles more accurately, and in part because there is a large uncertainty in the mass.

4. Σ decays

Three spin-$\frac{1}{2}$ Σ decays are listed in Table XXI, and one spin-$\frac{1}{2}$ Σ decay in Table XXII. Since we know only two out of the three θ_Σ mixing angles for both the spin-$\frac{1}{2}$ and spin-$\frac{3}{2}$ Σ's (see Tables VIII and XVI), we know the orientation in the three-dimensional mixing space for only one spin-$\frac{1}{2}$ Σ [the $\Sigma(1750)$] and only one spin-$\frac{3}{2}$ Σ [the $\Sigma(1670)$]. We therefore cannot make any predictions concerning the spin-$\frac{1}{2}$ $\Sigma(1620)$, or the three unobserved Σ states.

In Table XXII, fit No. 2 for the spin-$\frac{3}{2}$ Σ does not appear to be acceptable; the $\Sigma(1670) \to \Sigma^* \pi$ branching fraction, combined with the branching fractions in Table XII, yields a sum greater than unity. Fit No. 1, however, is consistent with the data available from the PDG.

[1] See, for example, N. Isgur and G. Karl, Phys. Rev. D **18**, 4187 (1978).

[2] R. Dashen and A. Manohar, Phys. Lett. B **315**, 425 (1993); **315**, 438 (1993); E. Jenkins, *ibid.* **315**, 431 (1993); **315**, 441 (1993); **315**, 447 (1993); R. Dashen, E. Jenkins, and A. Manohar, Phys. Rev. D **49**, 4713 (1994).

[3] Results that are closely related to those of Dashen, Jenkins, and Manohar (DJM) have been derived previously by various groups [4,5]. We focus on the work of DJM because the results are expressed in a language that can be simply related to the NRQM.

[4] J.-L. Gervais and B. Sakita, Phys. Rev. Lett. **52**, 527 (1984); Phys. Rev. D **30**, 1795 (1984).

[5] M.P. Mattis and M. Mukerjee, Phys. Rev. Lett. **61**, 1344 (1988); M.P. Mattis and E. Braaten, Phys. Rev. D **39**, 994 (1989); **39**, 2737 (1989).

[6] C. Carone, H. Georgi, and S. Osofsky, Phys. Lett. B **322**,

227 (1994).

[7] M. Luty and J. March-Russell, Report No. LBL-34778, 1993 (unpublished).

[8] E. Witten, Nucl. Phys. **B160**, 57 (1979). See also G. Adkins, C. Nappi, and E. Witten, *ibid.* **B228**, 552 (1983); A. Manohar, *ibid.* **B248**, 19 (1984).

[9] D. Faiman and D. Plane, Nucl. Phys. **B50**, 379 (1972); A. Hey, P. Litchfield, and R. Cashmore, *ibid.* **B95**, 516 (1975).

[10] F.J. Gilman, M. Kugler, and S. Meshkov, Phys. Lett. **45B**, 481 (1973); Phys. Rev. D **9**, 715 (1974).

[11] J.T. Donohue, Phys. Rev. Lett. **58**, 3 (1987); Phys. Rev. D **37**, 631 (1988).

[12] Particle Data Group, K. Hikasa *et al.*, Phys. Rev. D **45**, S1 (1992).

[13] See the review by T. Barnes, "The Status of Molecules," Report No. ORNL-CCIP-94-08, RAL-94-056, hep-ph/9406215 (unpublished).